Improving assessment of population exposure and health impacts to PM$_{2.5}$ with high spatial and temporal data

Xia Zhao, Yuyu Zhou, Xi Li, Tao Zhang, Yueying Wang, Zhengyuan Zhu, Kai Zhang & Deren Li

View supplementary material

Published online: 09 Aug 2024.

Submit your article to this journal

Article views: 710

View related articles

View Crossmark data

Taylor & Francis
Taylor & Francis Group

Improving assessment of population exposure and health impacts to PM$_{2.5}$ with high spatial and temporal data

Xia Zhao[a], Yuyu Zhou[b], Xi Li[c], Tao Zhang[d], Yueying Wang[e], Zhengyuan Zhu[e], Kai Zhang[f] and Deren Li[c]

[a]School of Public Administration, Zhejiang University of Finance and Economics, Hangzhou, China; [b]Department of Geography, The University of Hong Kong, Hong Kong, China; [c]State Key Laboratory of Information Engineering in Surveying, Mapping and Remote Sensing, Wuhan University, Wuhan, Hubei, China; [d]School of Resources and Environment, University of Electronic Science and Technology of China, Chengdu, China; [e]Department of Statistics, Iowa State University, Ames, IA, USA; [f]Department of Environmental Health Sciences, School of Public Health, University at Albany, Rensselaer, NY, USA

ABSTRACT

Exposure to ambient fine particulate matter (PM$_{2.5}$) poses a significant global health challenge. However, a major obstacle for epidemiological studies and risk assessment lies in the absence of high-resolution spatiotemporal exposure estimates. Here, we present an integrated framework to achieve accurate estimations of population exposure to PM$_{2.5}$ and assess related health risks by incorporating high temporal (hourly) and high spatial (1-km) PM$_{2.5}$ concentrations and population density, using Beijing, China, in 2015 as an example. Firstly, hourly PM$_{2.5}$ concentrations were estimated using a functional data model by integrating the gap-filled satellite-based aerosol optical depth data at 1-km resolution with hourly in-situ PM$_{2.5}$ observations. Then, we calculated the population-level exposure to PM$_{2.5}$ and associated health impacts incorporating both hourly PM$_{2.5}$ and population information. We also investigated the bias of exposure and health impact assessment using coarse spatial or temporal PM$_{2.5}$ and population data. Our findings revealed that exposure to PM$_{2.5}$ resulted in 33,830, 21388, and 5,302 premature deaths in 2015 attributable to all-cause, cardiovascular, and respiratory diseases, respectively. A sensitivity analysis conducted underscored the critical importance of considering the high spatiotemporal heterogeneity of both PM$_{2.5}$ concentrations and population density when investigating population-level PM$_{2.5}$ exposure and related health impacts. Insights on more accurate PM$_{2.5}$ exposure assessment from this study can help policymakers better assess improvements after clean air actions and analyze exposure inequality, and thereafter develop more effective pollution mitigation strategies.

1. Introduction

In recent decades, people have started monitoring ambient fine particulate matter with an aerodynamic diameter of less than 2.5 μm (PM$_{2.5}$) and understanding its health impacts (Brauer et al. 2016; Z. Chen et al. 2019; X. Li et al. 2021; Pisoni et al. 2023; Pope and Dockery 2006). Exposure to PM$_{2.5}$ has been attributed to approximately 4.2 million deaths globally in 2015 (Burnett et al. 2018; Stanaway et al. 2018). These inhalable fine particles can penetrate deeply into the lungs and circulation system, and cause adverse health effects (Cao et al. 2014; Krittanawong et al. 2023; Mebrahtu et al. 2023; Shi et al. 2021), such as all-cause (T. Li, Zhang, et al. 2018; Orellano et al. 2020), cardiovascular (Du et al. 2016; Hayes et al. 2020), and respiratory-related (Hamra et al. 2014; Turner et al. 2011) mortalities. The threat of PM$_{2.5}$ is particularly

concerning in developing countries (Lim et al. 2020; Tomar et al. 2023), such as China (Liu et al. 2021; Sun et al. 2023; P. Yin et al. 2020), owing to the rapid industrialization and urbanization fueled by fossil fuels in the past few decades (Gong et al. 2020; X. Li et al. 2020; Lu et al. 2020; Zhou et al. 2018). The World Bank (WB 2017) reported that more than 80% of the population in China lived in areas with PM$_{2.5}$ concentrations exceeding the WHO Interim Target I (35 μg/m^3/year) from 2010 to 2017. Previous studies estimated that approximately 1 million deaths per year were associated with PM$_{2.5}$ pollution in China (G. Yang et al. 2013; Yue et al. 2020).

Accurate estimation of the population exposure to ambient PM$_{2.5}$ is a prerequisite to address this public health issue. Studies have demonstrated that the health impact assessment of PM$_{2.5}$ is sensitive to the

spatial resolutions of PM$_{2.5}$ and population data (H. Bai et al. 2023; Fenech et al. 2018; Parvez and Wagstrom 2020; Xiao et al. 2021), especially for regions with obvious spatial variations of PM$_{2.5}$ (H. Bai et al. 2022). Such studies usually estimated related health impacts by using PM$_{2.5}$ and population data with various spatial resolutions ranging from several to a hundred kilometers based on annual mean population-weighted PM$_{2.5}$ exposure models and concentration-response (C-R) functions. Their findings illustrated the coarse spatial resolutions of data can bring over- or under-estimations for the final assessment results for different regions, compared with data in high spatial resolutions (e.g. 1 km), which are thought to characterize more spatial variations of PM$_{2.5}$ or population (H. Bai et al. 2023; Korhonen et al. 2019; Xiao et al. 2021). Accurate information on PM$_{2.5}$ and population dynamics is also critical for characterizing PM$_{2.5}$ exposure and assessing corresponding health effects, given the reality that both the high-frequency spatiotemporal variations of PM$_{2.5}$ concentrations and human activities are observed. For example, studies have demonstrated the significant diurnal changing patterns of PM$_{2.5}$ based on monitoring data (R. Li et al. 2015; Manning et al. 2018; Zhao et al. 2009); a significant spatiotemporal variation has also been detected in population density based on high-frequency location-based service (LBS) big data (Gariazzo, Pelliccioni, and Bolignano 2016; Nyhan et al. 2016; Zhao et al. 2021). Some efforts have been made by using input datasets with relatively higher temporal resolutions (e.g. monthly, 3-h) (B. Chen et al. 2018; Y. Song et al. 2019). However, such studies failed to simultaneously consider data at fine spatial and temporal scales, which do not consider the spatial variabilities of PM$_{2.5}$ (B. Chen et al. 2018) or the diurnal changes of PM$_{2.5}$ and population (Y. Song et al. 2019).

Due to limitations in simultaneously acquiring reliable PM$_{2.5}$ and population data with high temporal frequency (e.g. hourly) and sufficient spatial details, accurate estimates of population exposure to PM$_{2.5}$ are still lacking, and uncertainties caused by spatiotemporal resolutions of input datasets have still not been fully discussed. As for PM$_{2.5}$ concentration used in related studies, two strategies are usually used to map the spatial contiguous distributions of PM$_{2.5}$. One strategy is deriving PM$_{2.5}$ concentrations with high temporal resolution from the spatial interpolation of sparse station monitoring data, while these studies are not adequately considering the sufficient spatial heterogeneity of PM$_{2.5}$ distribution (B. Chen et al. 2018; Park and Kwan 2017; Steinle, Reis, and Sabel 2013; Xu et al. 2019). The other strategy is incorporating remote sensing auxiliary data with station observations, such as the widely used satellite-retrieved aerosol optical depth (AOD) data (Shin et al. 2020; X. Wang et al. 2020; J. Wei et al. 2021) and various statistical prediction models (e.g. multiple linear regression, linear mixed-effects model, geographically weighted regression model, and machine learning-based model) have been developed (H. Bai et al. 2023; He and Huang 2018; Ma et al. 2016; Zheng et al. 2020). The most widely used AODs were the Moderate Resolution Imaging Spectroradiometer (MODIS) carried by the Earth Observing System (EOS) satellites (i.e. Terra and Aqua), and numerous models were developed for daily PM$_{2.5}$ estimations. However, these models still have limitations in uncovering the high spatiotemporal variations of PM$_{2.5}$, owing to the limited temporal resolution of MODIS AOD data only twice daily (10:30 and 13:30 local time). The advent of geostationary satellite AOD data from Himawari-8 has improved the estimation of hourly PM$_{2.5}$ concentrations. However, the application of Himawari-8 AOD data in health impact analysis is still limited due to substantial data gaps. Therefore, the input PM$_{2.5}$ datasets in health impact analysis are just derived from limited hours of a day and are unable to reflect the high temporal PM$_{2.5}$ variations (H. Bai et al. 2023; Y. Song et al. 2019; Yue et al. 2020). As for population data, despite the enrichment of LBS big data allowing for more temporally resolved population distributions (Deville et al. 2014; Tsou et al. 2018), the temporal resolutions of population data used in health impact analysis are still coarse (e.g. yearly static, monthly, 3-h) (Beckx et al. 2009; B. Chen et al. 2018; Nyhan et al. 2016; Y. Song et al. 2019).

Therefore, estimating population exposure and health impacts of PM$_{2.5}$ at simultaneously finer spatial and temporal scales, which can more accurately delineate the real exposure situations and assess mitigation strategies, still remains challenging. To fill this gap, we present an integrated strategy to achieve high-resolution estimations of population exposure to PM$_{2.5}$ and assess related health impacts by incorporating hourly PM$_{2.5}$ and population information at

1-km resolution, using Beijing as an example. Second, we investigate uncertainties in the exposure levels and health impact assessments based on experiments using datasets at coarse spatial (e.g. population data at administrative level, $PM_{2.5}$ from spatial interpolation of only sparse station monitoring data) or temporal (daily mean from limited hours of derived $PM_{2.5}$) resolutions. The remainder of this paper is organized as follows. Section 2 describes the case study area and datasets used. In Section 3, data pre-processing and methodologies for mapping hourly ambient $PM_{2.5}$ concentrations as well as assessments of population exposure and health impacts associated with $PM_{2.5}$ are described. We present the results in Section 4, discussion in Section 5, and conclusions in Section 6.

2. Study area and materials

2.1. Study area

We used Beijing, the capital of China, as a case study area, which has suffered from frequent heavy $PM_{2.5}$ pollution episodes over the past decades. Beijing is located in the North China Plain, with an administrative area of 16,411 km^2 (Figure 1), and is the second-most populous city in China after Shanghai, with a population of 21.705 million in 2015. The annual mean $PM_{2.5}$ concentration in this region during 2015

was 83 μg/m^3 (range, 3 – 976 μg/m^3). It is approximately 16 times higher than the annual mean guideline value of 5 μg/m^3 recommended by the WHO air quality guidelines (AQGs) 2021 and 5 times higher than China's National Ambient Air Quality Standard Level I (MEEPRC 2016), indicating a high health risk. In addition, the $PM_{2.5}$ and population in Beijing show high-frequency spatiotemporal variations (K. Bai et al. 2020; Zhao et al. 2021), indicating it is an ideal region to evaluate uncertainties caused by the spatiotemporal resolutions of input datasets.

2.2. Ground-level $PM_{2.5}$ data

Hourly ground-level $PM_{2.5}$ observations at 35 stationary monitoring stations in 2015 (Figure 1) were collected from the Beijing Municipal Environmental Monitoring Center (BMEMC, http://zx.bjmemc.com. cn) to estimate the hourly spatially contiguous $PM_{2.5}$ concentrations across the Beijing region. The ambient $PM_{2.5}$ concentrations were measured using the tapered element oscillating microbalance (TEOM) or β-attenuation approaches with strict quality control procedures according to the HJ/T 193–2005 (https://www.cnemc.cn/jcgf/dqhj/200801/t20080129_647270.shtml.) and HJ 653–2013 (https://www.mee.gov.cn/ywgz/fgbz/bz/bzwb/jcffbz/201308/t20130802_256852.shtml)
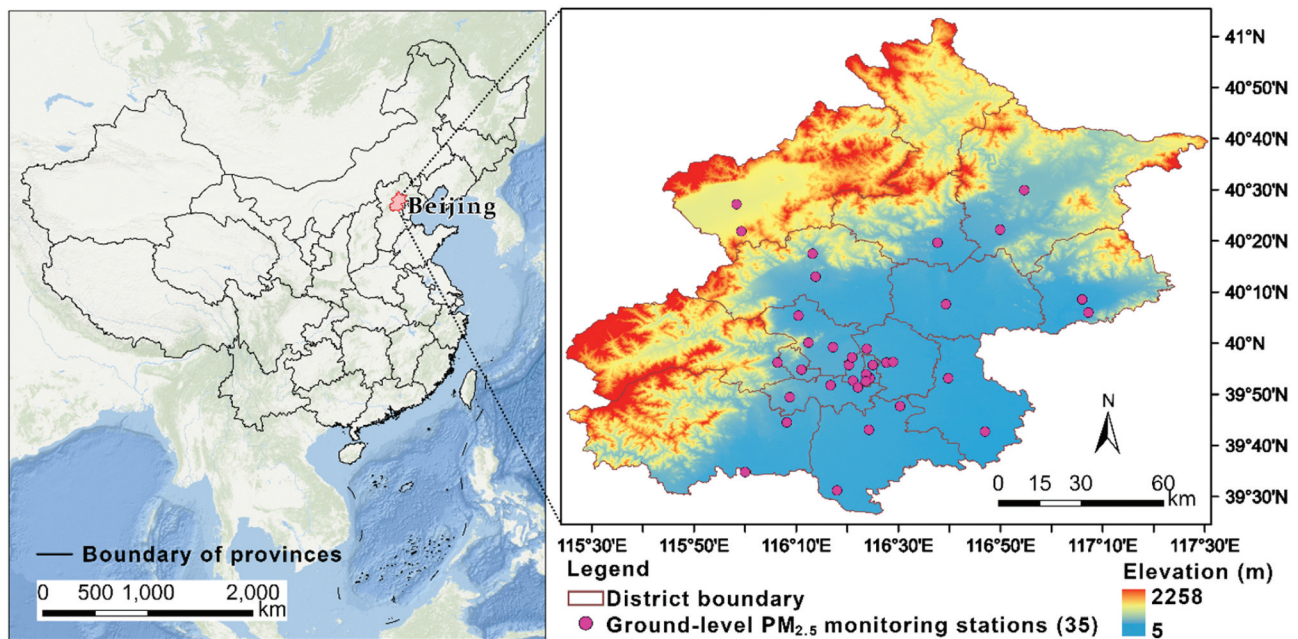

Figure 1. Study area of Beijing, China, and $PM_{2.5}$ monitoring stations. Elevation is SRTM version 4 data downloaded from https://srtm.csi.cgiar.org/srtmdata/.

standards published by the Ministry of Ecology and Environment of the People's Republic of China. These included regularly checking and correcting the related measurement parameters of automated monitoring equipment, and comparing the automatic measurement results to the manual monitoring data (as true value) to ensure the reliability of PM$_{2.5}$ observations.

2.3. MODIS AOD data

We collected AOD (MCD19A2) data from the Terra (~10:30) and Aqua (~13:30) satellites in 2015 at a resolution of 1 km. This product was generated by the multi-angle implementation of the atmospheric correction (MAIAC) algorithm from the darkest to the brightest surfaces at 550 nm (Lyapustin and Wang 2018). The MAIAC AOD data are superior for revealing numerous hotspots of high AOD values at fine scales and show better accuracy than other MODIS AOD products, such as MODIS Dark-Target (DT) and Deep-Blue (DB)-based products (Tao et al. 2019). MAIAC AOD retrievals demonstrated high accuracy and low estimation errors in mainland China compared with *in-situ* records from AERONET monitoring stations (J. Wei et al. 2020).

2.4. Dynamic population data

The dynamic population used in this study was from Zhao et al. (2021), in which a spatiotemporal downscaling framework was used to map hourly population dynamics by integrating remote sensing (e.g. land cover, and nighttime light data) and geospatial data (e.g. LBS data, points of interest data, and road network). The framework consists of three key steps: 1) generating population maps during sleep time and work time as baselines, 2) identifying urban functional zones for various activity types and detecting the corresponding human activity patterns, and 3) deriving hourly population distributions based on baseline populations and human activity patterns in urban functional zones. The derived population dynamics accurately captured the diurnal variability and spatial heterogeneity of the population in Beijing, providing essential information for assessing population exposure to PM$_{2.5}$.

2.5. Mortality and population database

The total (all-cause) mortality and the incidences of mortality data for different health endpoints (i.e. cardiovascular and respiratory diseases) were obtained to estimate the health impact attributed to PM$_{2.5}$. The total mortality and entire population of Beijing in 2015 were obtained from the China Statistical Yearbook published by the National Bureau of Statistics of China (NBSC, https://www.stats.gov.cn/sj/ndsj/2016/indexeh.htm). The incidences of mortality caused by cardiovascular and respiratory diseases were obtained from the Health Statistical Yearbook in 2015 published by the Beijing Institute of Hospital Management (BIHM, http://www.phic.org.cn/).

3. Methodology

We developed a framework, including data preprocessing (e.g. imputation of AOD data) and estimation of hourly ambient PM$_{2.5}$ concentrations as well as assessments of population exposure and associated health impacts (Figure 2). The details of this are described in the following sections.

3.1. Data preprocessing

3.1.1. Temporal interpolation of ground-level monitoring data

The PM$_{2.5}$ time series observed by monitoring stations presented missing records due to technical issues, such as instrument malfunction and power and internet outrages (K. Bai et al. 2020). For example, 96% of the days in 2015 in our study area had missing hour-level data. Given the evident diurnal patterns of ambient PM$_{2.5}$ concentrations demonstrated in previous studies (R. Li et al. 2015; Manning et al. 2018), we employed the diurnal-cycle-constrained empirical orthogonal function (DCCEOF) model (K. Bai et al. 2020) to interpolate the missing values. This model restored the missing values based on the initial hourly records and the reconstructed diurnal variation pattern derived from the corresponding neighborhood information in space and time. The detailed process and evaluation of the performance of this interpolated method are provided in the Supplementary Material S1. All the accuracy evaluation strategies reached above 0.90,
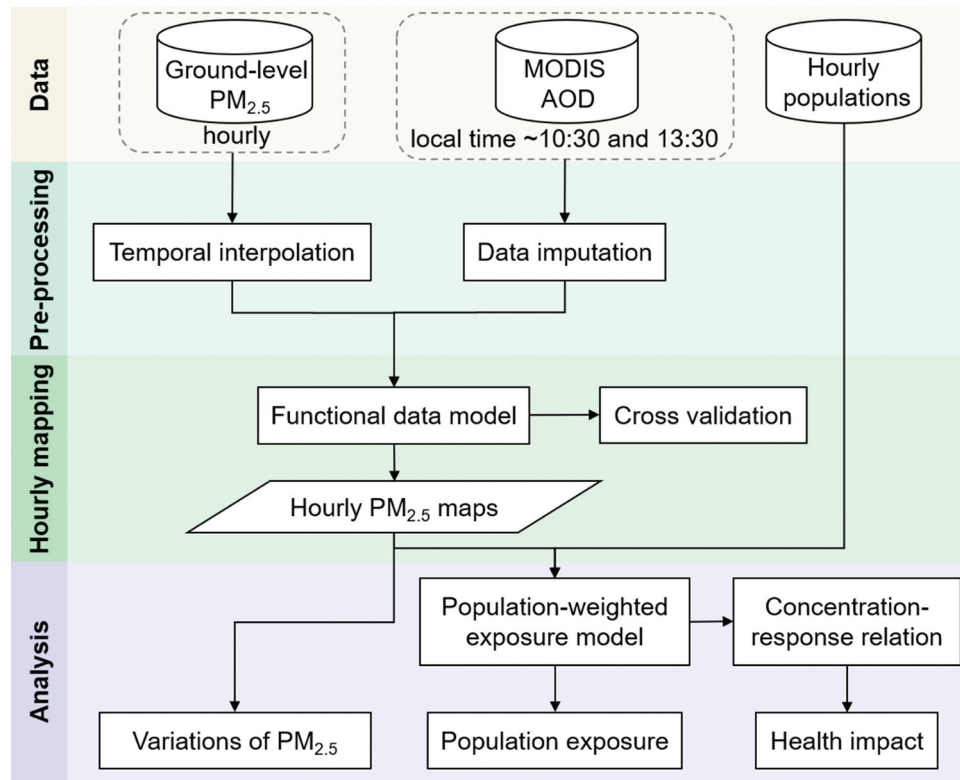
Figure 2. The framework to investigate PM$_{2.5}$ exposure and health impacts.

which can sufficiently support further hourly PM$_{2.5}$ mapping.

3.1.2. Imputation of AOD data

Due to geographical conditions (i.e. mountain terrains) and environmental factors (i.e. clouds, and high surface reflectance), there are spatial and temporal gaps regarding satellite-retrieved AOD data. Many strategies have been proposed to improve this problem, such as data-fusion methods based on multi-sourced AODs (Pu and Yoo 2022; Wei et al. 2021), and spatial statistical modeling (T. Zhang et al. 2022). In this study, we adopted the spatial statistical modeling strategy to fill the gaps in AOD data from the Terra and Aqua satellites based on temporal and spatial patterns of observed AODs (T. Zhang et al. 2022). This spatiotemporal imputation method can address the nonlinearity and non-stationary in temporal as well as consider the auto-correction in spatial with high efficiency and good performance. First, a cubic smoothing spline function was used to fit the long-term trend values (overall mean) based on the observations of each pixel (ordered by day of the year) with a smoothing parameter of 1 to obtain a continuous temporal trend for

each target pixel. If the start or end day of a year had no valid observation, we set its value as the 5% quantile of the time series values of the whole year. Second, the residuals between the observations and the overall means for each day with missing data were interpolated based on the correlation between the target pixel and its neighboring pixels. Finally, the missing AOD values were calculated by summing the overall mean and interpolated residuals with no missing values. For the flowchart of the imputation process, please refer to Figure S3. More detailed information regarding this spatiotemporal imputation algorithm can be found elsewhere (T. Zhang et al. 2022).

3.2. Mapping hourly PM$_{2.5}$ concentration

We applied a functional data model to map hourly PM$_{2.5}$ concentrations by integrating twice-a-day gap-filled AOD from satellites and hourly PM$_{2.5}$ observations from stations. The functional data fusion model proposed by Y. Wang (2021) was adopted with high computation efficiency. This model can take advantage of both spatially dense and temporally sparse AOD data and spatially sparse and temporally dense

PM$_{2.5}$ data, in which the AOD and PM$_{2.5}$ data at different time points were modeled as realizations of two-dimensional functions with a mean component and a stochastic component. For the flowchart of the modeling process, please refer to Figure S4. The mean functions described the overall spatial patterns of AOD and PM$_{2.5}$, which were temporally invariant functions of spatial locations, while the stochastic parts reflected the random variations of AOD and PM$_{2.5}$. Due to the spatially sparse distribution of monitoring stations, the spatial contiguous mean component of PM$_{2.5}$, which was difficult to estimate from ground observations alone, was estimated from that of spatial contiguous AOD by assuming a linear relationship between their means. The linear relationship was built based on the AOD and PM$_{2.5}$ at monitoring stations, and then extended to the entire study area. Thereafter, additional spatial covariance structure information was extracted from AOD and then combined with PM$_{2.5}$ observations at each time point to predict the stochastic component at all locations based on the functional principal component analysis (FPCA). The basic rationale behind the analysis is that there is a strong similarity between the spatial covariance functions of these two datasets (Y. Wang 2021).

We implemented the functional data model to estimate gridded hourly PM$_{2.5}$ concentration with the following steps: (1) estimating the mean function and covariance function of AOD based on the 1-km twice a day gap-filled AOD data using bivariate splines over triangulations (Lai and Wang 2013) and conduct FPCA (Y. Wang 2021; Y. Wang et al. 2020); (2) estimating the functional relationship between AOD and PM$_{2.5}$ based on the estimated mean function and covariance function of AOD and PM$_{2.5}$ time series data at stations using maximum likelihood estimators under Gaussian assumption; (3) estimating the mean function and covariance function of PM$_{2.5}$ based on the mean function and covariance function of AOD estimated in step (1) and the relationship estimated in step (2); (4) conducting FPCA and obtaining eigenvalue as well as corresponding eigenfunctions based on the estimated covariance function; (5) predicting the functional principal component scores of the stochastic component in PM$_{2.5}$ at specific time points considering the ground-level observations at these time points and the estimated covariance structure; (6) adding the spatial contiguous mean and the

predicted stochastic components to get 1-km spatial resolution hourly PM$_{2.5}$ concentration. We resampled the hourly spatial contiguous PM2.5 concentration into a 500-m resolution by using the nearest neighbor interpolation strategy.

Thereafter, we adopted two 10-fold cross-validation (CV) techniques (i.e. sample-based and station-based CV) to evaluate the reliability of the model for hourly PM$_{2.5}$ mapping by comparing the estimations at grids with stations with corresponding ground-level station records (T. Li, Shen, et al. 2018; X. Wang et al. 2020). The sample-based and station-based CVs were used to evaluate the overall prediction ability and spatial prediction performance of the model, respectively. Finally, three statistical metrics, namely determination coefficient (R^2), root-mean-square error (RMSE, μg/m^3), and mean absolute error (MAE, μg/m^3) were used to indicate the CV accuracy of the model (Supplementary Material S2).

3.3. Population-weighted exposure assessment

Given the simultaneous changes in population and PM$_{2.5}$ concentration over time, we used a population-weighted exposure model to estimate the population exposure to ambient PM$_{2.5}$ at multi-temporal scales (H. Bai et al. 2023; Nyhan et al. 2016; Y. Song et al. 2019). At the city level, we assessed hourly PM$_{2.5}$ exposure for each day by synthesizing all grid cells using Equation (1). Thereafter, we sequentially estimated the monthly mean and annual mean exposure for each hour.

$$E_{d,h} = \frac{\sum_{i=1}^{n} (Pop_{i,d,h} \times PM_{i,d,h})}{\sum_{i=1}^{n} Pop_{i,d,h}} \quad (1)$$

where $Pop_{i,d,h}$ and $PM_{i,d,h}$ refer to the population number and PM$_{2.5}$ concentrations for a specific grid cell during a given hour h of a given day d, respectively. h refers to the hours of the day, ranging from 0 to 23. $E_{d,h}$ denotes the population-weighted exposure in day d.

3.4. Health impact assessment

We estimated the annual premature mortalities associated with PM$_{2.5}$ using a health impact function based on a log-linear relationship between relative

risk (*RR*) and pollutant concentration, which links changes in PM$_{2.5}$ concentration with changes in mortality (Anenberg et al. 2010; Liang et al. 2020). *RR* captures the incidence of a certain health endpoint under the actual concentration (*C*) compared to that under the baseline concentration (*C$_0$*) (Equation (2)).

$$RR = e^{\beta(C-C_0)} = e^{\beta\Delta x} \qquad (2)$$

where β denotes the concentration-response factor (i.e. the slope of the log-linear relationship between concentration and mortality), and ΔX is the change in PM$_{2.5}$ concentrations. The concentration baseline of PM$_{2.5}$ (*C$_0$*) was defined according to the WHO recommendation for good health (i.e. 10 μg/m^3/year). The actual PM$_{2.5}$ concentration (*C*) was the calculated annual mean population-weighted PM$_{2.5}$ exposure level in Beijing.

Based on the definition of relative risk, the fraction of the disease burden attributable to PM$_{2.5}$, i.e. the attributable fraction (*AF*), is defined in Equation (3). Thereafter, the total PM$_{2.5}$-attributed premature deaths (*ΔMort*) were estimated based on the baseline mortality rate (*y$_0$*) and the size of the exposed population (*Pop*) using Equation (4).

$$AF = \frac{RR - 1}{RR} = 1 - e^{-\beta\Delta x} \qquad (3)$$

$$\Delta Mort = y_0 \times AF \times Pop \qquad (4)$$

In this study, premature mortalities for three health endpoints (i.e. all-causes, cardiovascular, and respiratory diseases) attributed to PM$_{2.5}$ at all ages were estimated based on the population-weighted annual mean PM$_{2.5}$ concentrations. The entire population of Beijing was assumed to be exposed to the same PM$_{2.5}$ concentrations as the corresponding outdoor PM$_{2.5}$ concentrations (Y. Song et al. 2019) and the short-term RRs used in this study were derived from a local study over the Beijing region using over-dispersed generalized linear Poisson models at a daily scale (R. Chen et al. 2011). Specifically, a 10 μg/m^3 increase in PM$_{2.5}$ resulted in 0.53% (95% confidence interval [CI]: 0.37%, 0.69%), 0.58% (95% CI: 0.35%, 0.81%), and 0.66% (95% CI: 0.21%, 1.11%) increases in RRs for all-cause mortality, cardiovascular mortality, and respiratory mortality, respectively (without considering the lag effect). However, the lag health effects of PM$_{2.5}$ cannot be ignored, because current exposure and previous exposure to PM$_{2.5}$ have a combined impact on health (P. Li et al. 2022; Schwartz 2000) (Table S2). In addition, the baseline incidence rates (*y$_0$*) for different health endpoints and the exposed population (*Pop*) in 2015 were collected from the published mortality database and Beijing Statistical Yearbook described in Section 2.5.

3.5. Sensitivity analysis

To investigate uncertainties in health impact assessment caused by using coarse spatiotemporal PM$_{2.5}$ concentration and population data, eight

Table 1. Exposure experiments using coarser datasets.

Experiment*	Datasets		Description
	PM$_{2.5}$ concentration	Population distribution	
CS-CST	Hourly station-based PM$_{2.5}$	County-level demographic data	(1) **C**oarse **s**patial accuracy of PM$_{2.5}$; (2) **c**oarse **s**patio**t**emporal accuracy of population distribution
CT-CST	Daily satellite-derived PM$_{2.5}$	County-level demographic data	(1) **C**oarse **t**emporal accuracy of PM$_{2.5}$; (2) **c**oarse **s**patiotemporal accuracy of population distribution
IST-CST	Hourly satellite-derived PM$_{2.5}$	County-level demographic data	(1) **I**mproved **s**patio**t**emporal accuracy of PM$_{2.5}$; (2) **c**oarse **s**patiotemporal accuracy of population distribution
CS-CT	Hourly station-based PM$_{2.5}$	WorldPop data	(1) **C**oarse **s**patial accuracy of PM$_{2.5}$; (2) **c**oarse **t**emporal accuracy of population distribution
CT-CT	Daily satellite-derived PM$_{2.5}$	WorldPop data	**C**oarse **t**emporal accuracy of PM$_{2.5}$ and population distribution
IST-CT	Hourly satellite-derived PM$_{2.5}$	WorldPop data	(1) **I**mproved **s**patio**t**emporal accuracy of PM$_{2.5}$; (2) **c**oarse **t**emporal population distribution
CS-IST	Hourly station-based PM$_{2.5}$	Dynamic population data	(1) **C**oarse **s**patial accuracy of PM$_{2.5}$; (2) **i**mproved **s**patio**t**emporal accuracy of population distribution
IST-IST	Hourly satellite-derived PM$_{2.5}$	Dynamic population data	**I**mproved **s**patio**t**emporal accuracy of PM$_{2.5}$ and population distribution

*The naming rule for experiments: CST, CS, CT, and IST denote **c**oarse **s**patio**t**emporal accuracy, **c**oarse **s**patial accuracy, **c**oarse **t**emporal accuracy, and **i**mproved **s**patio**t**emporal accuracy. For example, CS-CST denotes an experiment based on the PM$_{2.5}$ concentration and population distribution in **c**oarse (C) **s**patial (S) accuracy and **c**oarse (C) **s**patio**t**emporal (ST), respectively.

exposure experiments were conducted using different datasets, and the corresponding health impacts were compared (Table 1). Two types of static populations, that is, at coarse spatiotemporal (e.g. -CST) and high spatial but coarse temporal (e.g. -CT) resolutions, were used at different spatiotemporal resolutions of PM$_{2.5}$ concentrations (e.g. station-based and satellite-derived, and daily and hourly). County-level demographic data were equally disaggregated into 500-m grids. The station-based PM$_{2.5}$ concentrations were interpolated into continuous surfaces at a 500-m resolution using the inverse distance weighting interpolation technique. In addition, to examine the uncertainties of health impact assessment caused by using the PM$_{2.5}$ concentration from limited hours (e.g. local time 10:30 and 13:30 based on MODIS AOD data), satellite-derived daily PM$_{2.5}$ concentrations were derived by averaging hourly PM$_{2.5}$ concentrations at nearby time-points (e.g. 10:00, 11:00, 13:00, and 14:00). The 100-m gridded static

population data for 2015 were downloaded from WorldPop (https://www.worldpop.org/) and aggregated into 500-m grids by summing the population counts inside a 500-m grid. In addition, we also estimate the attributable mortality using the Global Exposure Mortality Model (GEMM) proposed by Burnett et al. (2018) to investigate the impact of model selection (Supplementary S4).

4. Results

4.1. Evaluation of the hourly PM$_{2.5}$ estimations

The scatter plots show a good agreement between our estimated and observed PM$_{2.5}$ concentrations (Figure 3), indicating the reliability of the derived hourly PM$_{2.5}$ distributions using the functional data model. For example, R^2, RMSE, and MAE were approximately 0.87, 32 μg/m^3, and 16 μg/m^3, respectively, based on the sample-based CV (Figure 3(a)) and station-based CV (Figure 3(b)).
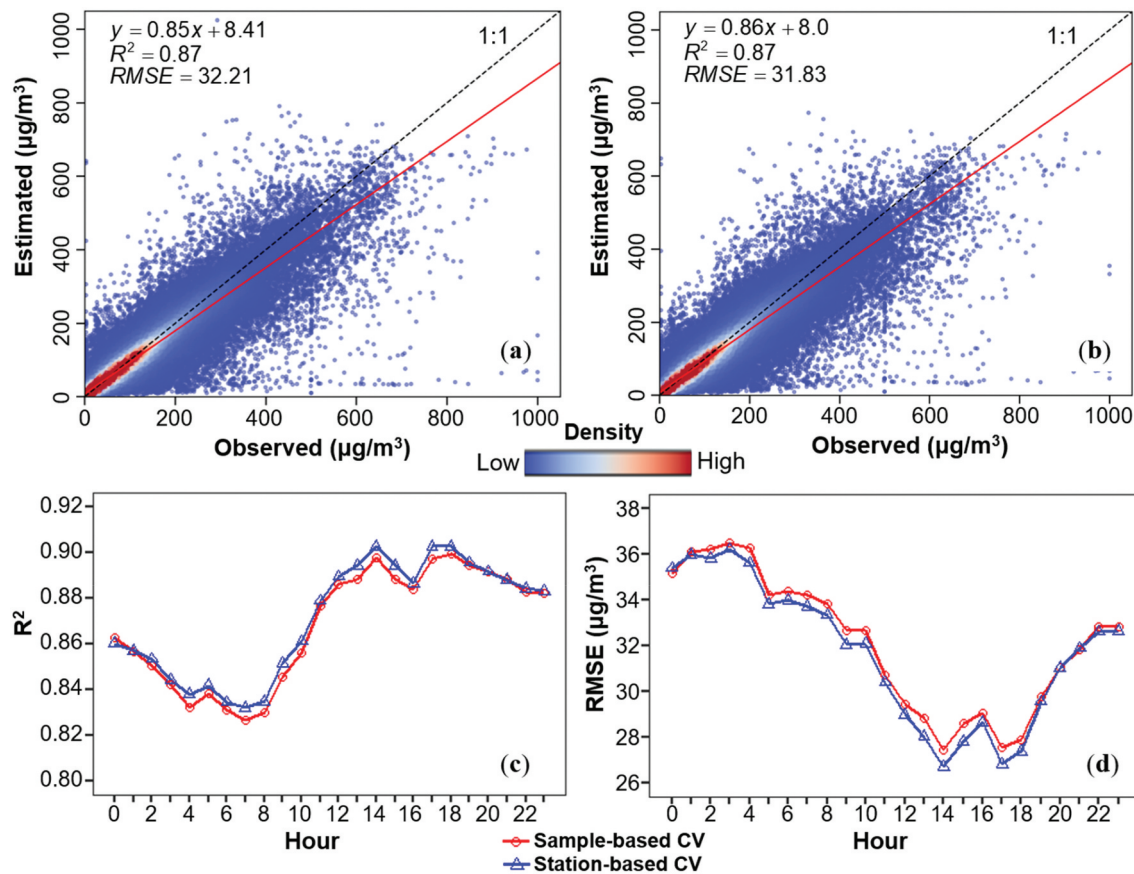

Figure 3. Evaluation of hourly PM$_{2.5}$ concentrations using the functional data model in Beijing in 2015. Ten-fold sample-based CV (a) and station-based CV (b) results; performances of R^2 (c) and RMSE (d) at each hour. CV is the abbreviation of cross-validation.

Figure 3(c,d) present the CV results at each hour and illustrate that the sample-based and station-based CV results were almost the same each hour. Although the CV results changed hourly, all R^2 values were higher than 0.82, with the highest of approximately 0.90 at 14:00, 17:00, and 18:00. The CV results also illustrate that the functional data model performed better during 10:00 – 23:00 than during 3:00 – 8:00 for estimating hourly $PM_{2.5}$ concentrations.

4.2. Variations in $PM_{2.5}$ concentrations

Significant spatiotemporal variation in $PM_{2.5}$ was found across Beijing (Figure 4). Explicit and similar geographic variations in $PM_{2.5}$ concentrations ($31 – 116 \, \mu g/m^3$) were observed, with more severe $PM_{2.5}$ pollution in the southeast plain than in the northwest mountainous region.

Significant diurnal variation in $PM_{2.5}$ concentrations was observed from 0:00 to 23:00 (Figure S7). The diurnal cycle shows a double falling-rising pattern as a "W"-shaped with peaks appearing during the early morning (0:00 – 5:00), noon (9:00 – 12:00), and nighttime (19:00 – 23:00), while the minimum occurred at the afternoon (14:00 – 17:00). The peak $PM_{2.5}$ concentration during nighttime ($71.34 \pm 18.55 \, \mu g/m^3$) was about 1.2 times higher than the afternoon concentration ($58.96 \pm 13.62 \, \mu g/m^3$). In addition, the annual mean $PM_{2.5}$ concentration in Beijing during 2015 varied from 34.30 to 104.91 $\mu g/m^3$ spatially with a mean value of 64.97 $\mu g/m^3$.

To better capture the temporal variation in hourly $PM_{2.5}$ concentrations, we further investigated changes in hourly $PM_{2.5}$ concentrations at the monthly scale, and the results illustrated significant changes in $PM_{2.5}$ concentrations among months (Figure 5). High $PM_{2.5}$ concentrations occurred during the winter and
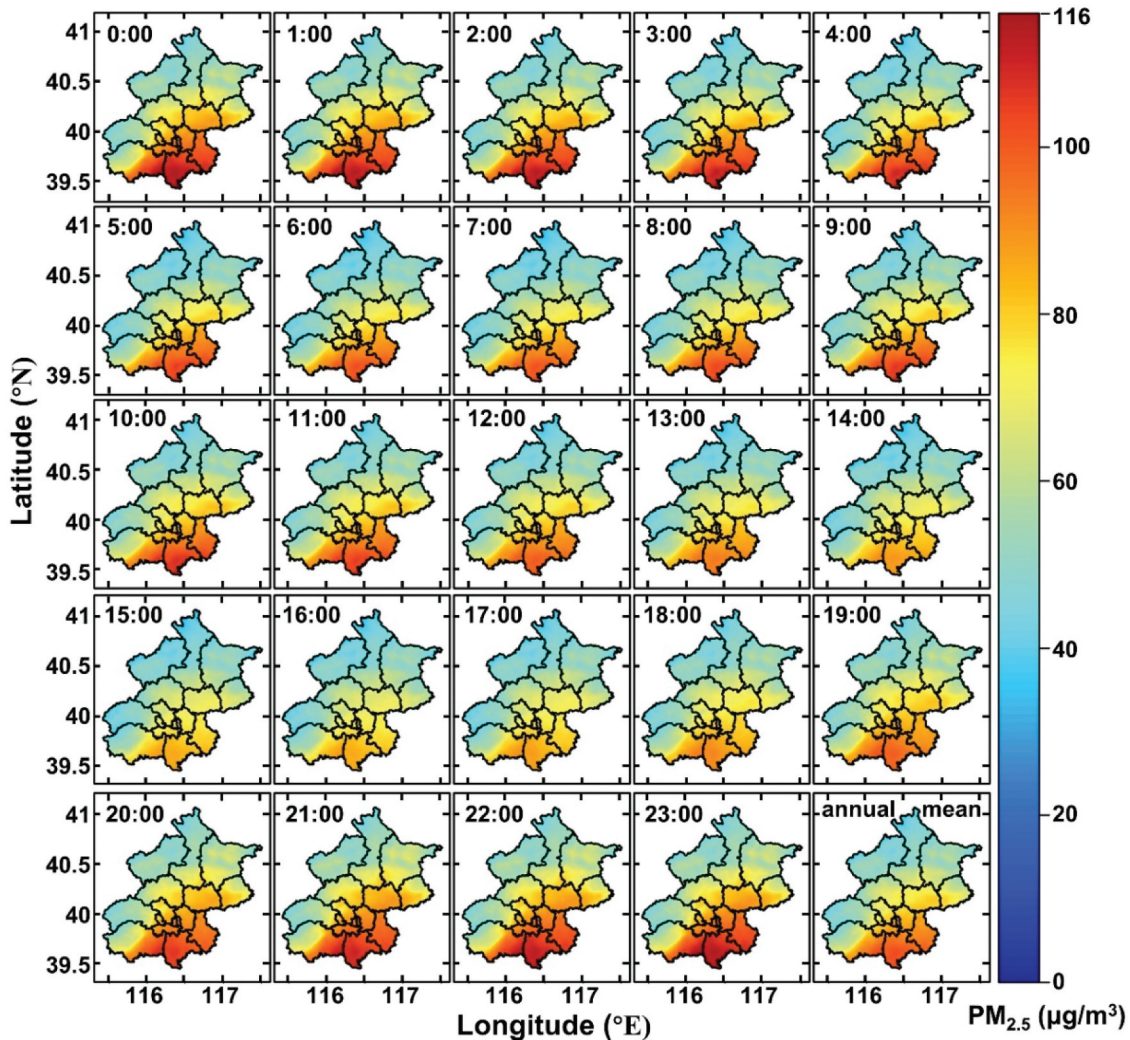

Figure 4. Hourly (0:00–23:00 local time) and daily mean $PM_{2.5}$ concentrations in Beijing in 2015.
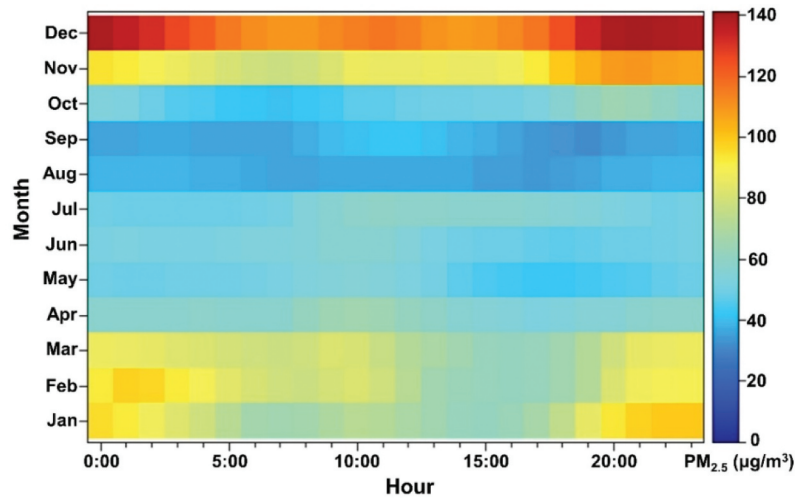
Figure 5. Temporal variation in hourly PM$_{2.5}$ concentrations in each month in Beijing in 2015.

reached the most severe level (108 – 140 µg/m^3) in December, which was mainly caused by the joint effect of meteorological conditions and the increasing demand of coal burning for heat (Q. Zhang et al. 2009). The PM$_{2.5}$ concentrations were relatively low during the late spring, summer, and early autumn, with the lowest concentration in August (36.61 – 38.70 µg/m^3) and September (31 – 41.98 µg/m^3). In addition, the temporal pattern of hourly PM$_{2.5}$ concentrations in the monthly profiles exhibited a similar "W"-shaped pattern in months (i.e. January to March, August, and December) with peaks in the early morning (0:00 – 3:00), morning (9:00 – 11:00) and nighttime (20:00 – 23:00), as well as an afternoon minimum between 14:00 and 16:00. The peak hourly PM$_{2.5}$ concentration from April to June and September was between 9:00 and 13:00, and the lowest was between 17:00 and 19:00. In addition, the hourly PM$_{2.5}$ concentration in July was highest during 10:00 – 20:00, which might be caused by the increase in human activities. At 6:00 – 10:00 during October and November, the PM$_{2.5}$ concentrations were the lowest, and the relatively high concentration occurred after 20:00.

4.3. Population exposure to PM$_{2.5}$

We found significant temporal variation in exposure by hour (Figure 6(a)) and further investigated whether
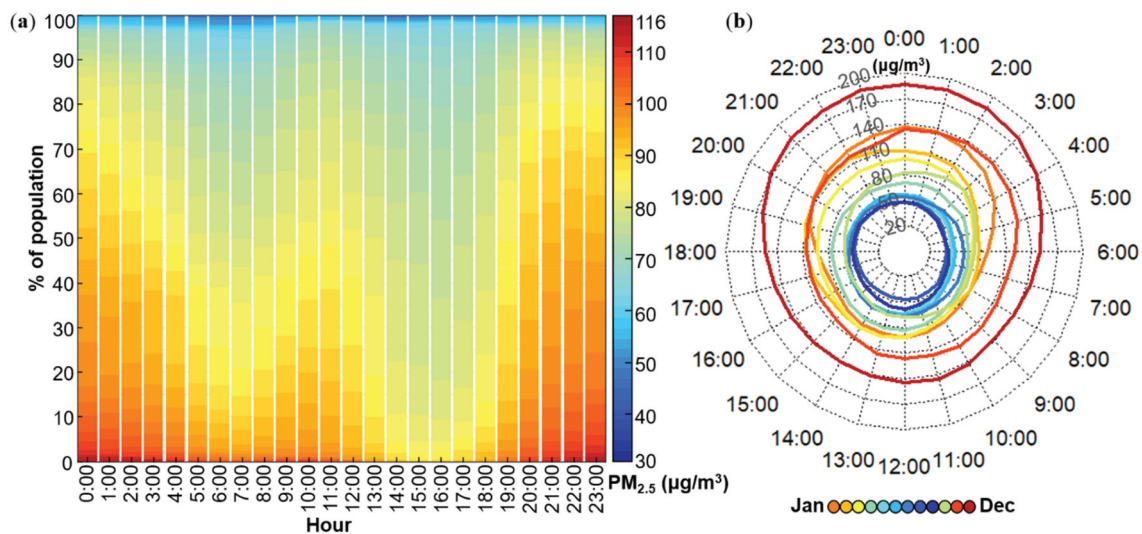

Figure 6. Cumulative percentage of population exposure to various PM$_{2.5}$ concentration levels (a) and temporal variation of hourly PM$_{2.5}$ exposure levels in each month (b) in Beijing in 2015.

the hourly exposure pattern also changed in the monthly profile (Figure 6(b)). The worst exposure conditions occurred during the early morning (0:00 – 5:00) and evening (19:00 – 23:00) periods, followed by noon (9:00 – 12:00) (Figure 6(a)). More than 50% of the population was exposed to a mean $PM_{2.5}$ concentration higher than 81 µg/m^3 (WHO Interim Target-1, 35 µg/m^3) during these periods. Between 14:00 and 17:00, the exposure condition improved, and more than 90% of the population was exposed to levels less than this concentration. Greater temporal variations in hourly population exposure levels were observed in 2015 (Figure 6(b)). Results show that November to December was the worst exposure period with peak exposure level in December (137.74 – 187.01 µg/m^3), followed by the period from January to February (77.23 – 136.38 µg/m^3). Decreased exposure levels were observed from June to September, with the lowest in August (38.87 – 50.24 µg/m^3). In general, the hourly population exposure levels in the monthly distribution can be divided into three patterns: "W"-shaped pattern, with peak exposure levels occurring during 0:00 – 5:00 and 21:00 – 24:00, and a small peak appearing between 11:00 and 16:00, including months of January to March, August, and October to December; "N"-shaped pattern, with the peak exposure level occurring during 10:00 – 15:00, and the valley exposure level during 18:00 – 21:00, including months of April-June and September; inverted "V"-shaped pattern, with the peak exposure level appearing during 10:00–15:00, for example, the month of July.

4.4. Sensitivity evaluation

We estimated the attributable premature deaths for the three health endpoints in eight exposure scenarios using different datasets, and the comparison showed a large disparity in the estimations between these experiments (Table 2). The total number of premature deaths attributed to short-term $PM_{2.5}$ exposure in the study area was 33,830 (95% CI: 25095 – 41,607) for all-cause 21,388 (95% CI: 13745 – 27,823) for cardiovascular disease, and 5,302 (95% CI: 1,247 – 8,070) for respiratory diseases in 2015 using both high spatiotemporal resolution data of $PM_{2.5}$ and population (IST-IST). The experiment using $PM_{2.5}$ data at coarse spatial resolution and population data at improved spatiotemporal resolution (CS-IST) showed the largest positive disagreement compared with the results of IST-IST with positive biases of 1422, 882, and 211 in all-cause, cardiovascular, and respiratory diseases, respectively. This is followed by an exposure scenario of using hourly station-based $PM_{2.5}$ and county-level demographic data (CS-CST) with a positive bias of 923, 573, and 137. In addition, all derived health burdens under the other five exposure scenarios underestimated the premature deaths attributed to $PM_{2.5}$. The estimation using coarse temporal $PM_{2.5}$ and population data (CT-CT) showed the largest negative disagreement with IST-IST of 4981, 3099, and 749 for all-cause, cardiovascular, and respiratory diseases, respectively. Additional experimental results considering a lag of day 1 for short-term RR parameters yielded similar difference

Table 2. Comparison of mean exposure levels and premature deaths from different exposure experiments.

Experiment	Mean exposure (µg/m^3/year)	Premature mortality*		
		All-cause	Cardiovascular	Respiratory
CS-CST	83.73	34,753 (25,823 – 42,675)	21,961 (14,148 – 28,502)	5,439 (1,286 – 8,239)
CT-CST	75.22	31,398 (23,191 – 38,776)	19,877 (12,692 – 26,015)	4,938 (1,144 – 7,613)
IST-CST	77.60	32,353 (23,937 – 39,892)	20,472 (13,104 – 26,729)	5,081 (1,184 – 7,794)
CS-CT	74.89	31,268 (23,089 – 38,624)	19,796 (12,636 – 25,918)	4,918 (1,139 – 7,588)
CT-CT	69.10	28,849 (21,214 – 35,781)	18,289 (11,601 – 24,087)	4,553 (1,039 – 7,114)
IST-CT	71.38	29,835 (21,976 – 36,943)	18,904 (12,021 – 24,837)	4,702 (1,079 – 7,309)
CS-IST	85.03	35,252 (26,218 – 43,251)	22,270 (14,367 – 28,866)	5,513 (1,308 – 8,329)
IST-IST	81.35	33,830 (25,095 – 41,607)	21,388 (13,745 – 27,823)	5,302 (1,247 – 8,070)

*Values in parentheses denote values within 95% confidence intervals (CI). Besides, in the Experiment column, the text before the horizontal bar refers to PM2.5 data, while the text after the horizontal bar refers to population data. CST, CS, CT, and IST denote coarse spatiotemporal accuracy, coarse spatial accuracy, coarse temporal accuracy, and improved spatiotemporal accuracy. The estimated RRs are 1.054 (95% CI: 1.038, 1.071), 1.060 (95% CI: 1.036, 1.084), and 1.068 (95% CI: 1.021, 1.117) for all-cause, cardiovascular, and respiratory, respectively. Note that the published mortalities for all-cause, cardiovascular, and respiratory are 107,440, 63114, and 14,117, respectively.

patterns (Table S2). Compared to the results from GEMM (Figure S8), we found that the estimation differences in the data used have a significantly greater impact than the model selection for all-cause results. For cardiovascular results, both data and model selections contribute to relatively large discrepancies. These findings underscore the critical importance of accurate $PM_{2.5}$ and population data inputs for health impact assessment.

5. Discussion

This study assessed population exposure and health impacts associated with ambient $PM_{2.5}$ concentrations by integrating high spatiotemporal $PM_{2.5}$ and population maps. Although previous studies have demonstrated the significant diurnal variation and spatial disparity of the $PM_{2.5}$ concentrations (R. Li et al. 2015; Manning et al. 2018) as well as the difference in population exposure within a day (Nyhan et al. 2016), only a few studies provide more detailed temporal information on population exposure. In this study, we filled this gap by assessing population exposure with a thorough consideration of population dynamics and spatiotemporal variations in $PM_{2.5}$ concentrations at the finest spatiotemporal resolutions.

Hourly $PM_{2.5}$ concentrations and population distribution across the study area can well reveal the temporal hotspots of population-level exposures caused by temporal variable factors (e.g. rush hours and weather conditions), which are hidden by using daily or coarser temporal data. The $PM_{2.5}$ concentrations changed drastically in a short time, as shown in the derived concentrations at 8:00, 16:00, and 22:00 local time (Figure 7(a)). The difference in $PM_{2.5}$ concentrations between hours in a day was higher than 200 μg/m^3, and large changes appeared in the highly polluted months of a year (e.g. January, February, and December), affected by the joint effect of the dry climate and heavy wind during this period (R. Li et al. 2015). However, previous studies on pollution exposure and environmental health impacts tend to assume the temporal constant of $PM_{2.5}$ concentration levels throughout a period of time (e.g. day, month, or year), due to the limited temporal resolution of derived $PM_{2.5}$ concentration data (Liang et al. 2020; C. Song et al. 2017; Y. Song et al. 2019). In this study, the derived daily mean $PM_{2.5}$ from limited hours could

not accurately capture the diurnal pattern of $PM_{2.5}$, showing a large bias of up to ±60 μg/m^3 compared with the daily mean results from all hours (Figure 7 (b)). Considering both dynamic population mobility and $PM_{2.5}$ fluctuation information, the estimated exposure level was 81.35 μg/m^3, which is about 10 μg/m^3 higher than the previous study that used monthly average population maps and limited-hour daily mean $PM_{2.5}$ concentrations for Beijing in 2015 (Y. Song et al. 2019).

The comparison (Table 2) indicates that the use of this limited-hour daily mean (CT-) underestimated health impacts compared with the hourly station-based and satellite-derived $PM_{2.5}$ (CS-CST, IST-CST and CS-CT, IST-CT) under the same population condition, which might be due to the fact that higher pollution levels usually occurred in the late night and early morning (Cheng et al. 2017; R. Li et al. 2015). In addition, the use of $PM_{2.5}$ data at coarse spatial resolution (CS-) led to the largest positive disagreement compared with other exposure scenarios (CT-CST, IST-CST, CT-CT, and IST-CT) at the same population distribution, which might be due to the fact that the $PM_{2.5}$ monitoring stations are mainly distributed in urban centers with higher pollution levels and the derived spatially contiguous $PM_{2.5}$ distribution by simple interpolation increased the overall exposure level. Results of using population data at the improved spatiotemporal resolution (–IST) show higher exposure levels compared to other population distributions, which might be due to the fact that people travel toward the city centers during work time (Zhao et al. 2021). Therefore, considering hourly spatiotemporal variations of $PM_{2.5}$ concentration and population distribution are needed in future related studies.

Although our proposed strategy provides an effective and reliable way to estimate $PM_{2.5}$ exposure and health impact, several potential biases and limitations remain. First, although the functional data model performed well in estimating hourly spatial continuous $PM_{2.5}$ concentrations, the sparse and uneven distribution of ground-level monitoring stations in the study area as well as the only used AOD data in this model might introduce biases. For example, topology, weather conditions, land use features, traffic conditions, and emissions are usually considered together with AOD to depict the spatial fluctuation of $PM_{2.5}$ more accurately (Miao et al. 2022; Xie et al. 2015;
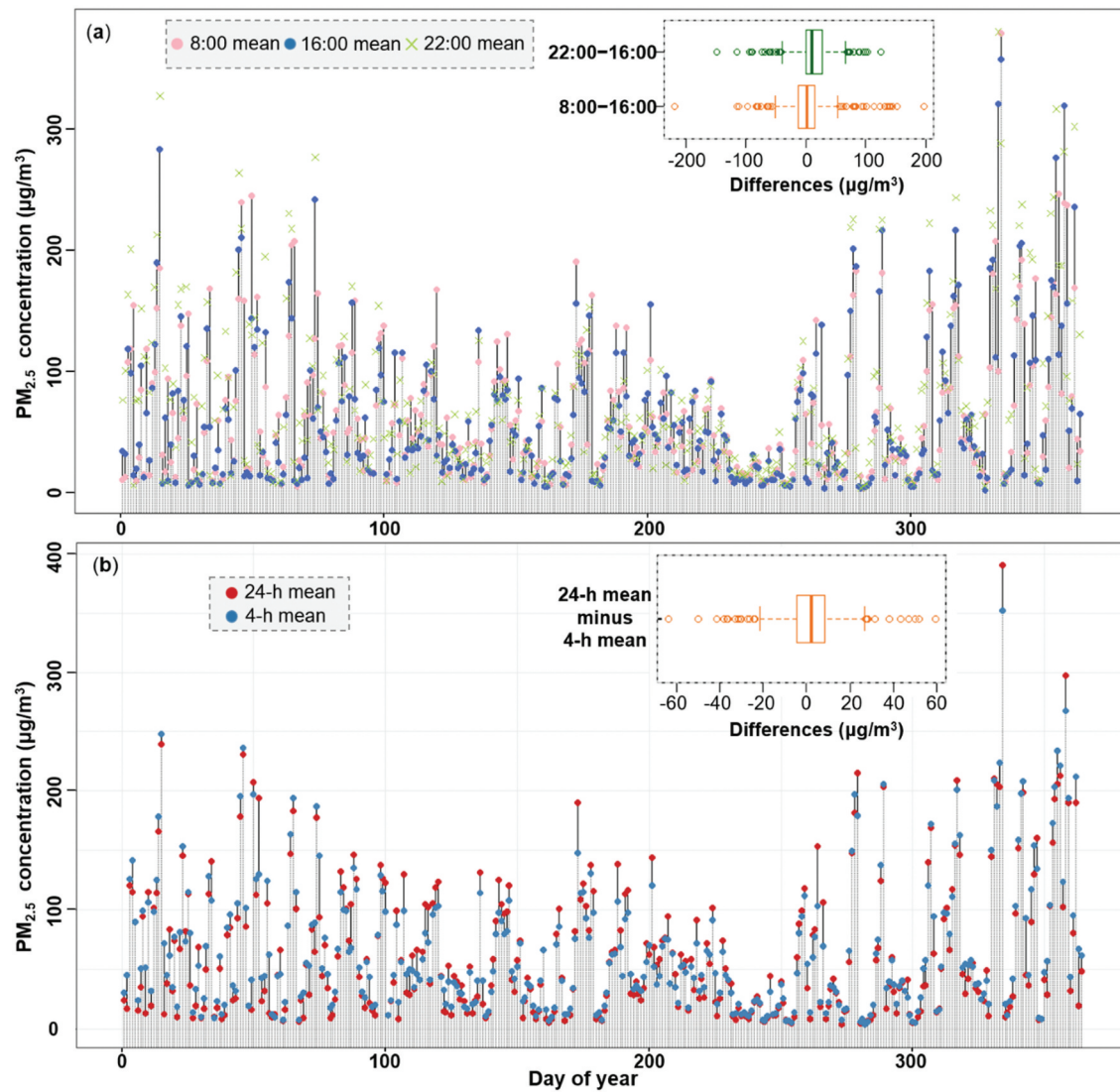
Figure 7. Temporal variations of PM$_{2.5}$ concentration. Example of the temporal variations of PM$_{2.5}$ concentration between selected hours (a) and differences of daily averaged PM$_{2.5}$ concentrations calculated by full-time (24-h) and limited-time (4-h) PM$_{2.5}$ concentrations in a day (b). Note that the limited-time PM$_{2.5}$ concentrations were calculated by averaging concentrations at 10:00, 11:00, 13:00, and 14:00 local time, to keep consistent with the estimated PM$_{2.5}$ concentrations limited at the temporal resolution from MODIS AOD data.

X. Zhang et al. 2018). Second, complex exposure and health feedback situations were not considered in this study (e.g. indoor exposure scenarios, age factors, and PM$_{2.5}$ constituents). Despite the assumption that all people at all times were exposed to the same PM$_{2.5}$ concentrations as the corresponding ambient PM$_{2.5}$ concentrations (H. Bai et al. 2023; Liang et al. 2020; Y. Song et al. 2019), the actual exposure for individual level is affected by both outdoor and indoor PM$_{2.5}$ concentrations. Indoor exposure might be diverse and complex, which was influenced by indoor activities (e.g. cooking), house standards, and outdoor pollutions (Dong et al. 2020). However, we adequately considered population dynamics for estimating PM$_{2.5}$

exposure and health impacts at a high spatiotemporal resolution compared with previous studies (Luo et al. 2020; Nyhan et al. 2016; Y. Song et al. 2019), the varied sensitivity of different population groups to the PM$_{2.5}$ level (H. Yin et al. 2021) was not considered because of the limited information from LBS data (e.g. social media data) to capture the dynamics of population subgroups (Y. Song et al. 2019). Owing to the complex and temporal variations of PM$_{2.5}$, its composition is difficult to distinguish. Population exposure to the same PM$_{2.5}$ levels, but with different constituents, might have different health impacts (Taj et al. 2020). Besides, limited by the access to related mortality rates, for example, publicly available disease mortality

rates are published taking Beijing as a total statistical region, the spatial difference between exposure level and mortality rates cannot be compared; the associated premature deaths were estimated based on mortality data on an annual basis without considering cumulative effects in short-term analysis, due to the limitations for acquiring the short-term mortalities.

6. Conclusions

In this paper, we presented an improved framework for the assessment of population exposure and health impacts using high spatiotemporal resolution data of $PM_{2.5}$ and population. The framework can be extended to larger geographical regions (e.g. national or continental), where relevant data are available. A comparison of eight exposure experiments demonstrated that coarse spatial or temporal resolution data of $PM_{2.5}$ concentration and population could lead to biases in the health impact assessment, indicating that high spatiotemporal information of $PM_{2.5}$ and population should be jointly considered in future studies. For example, future research on exposure and health impacts over a longer period can be explored using hourly $PM_{2.5}$ concentrations by integrating AOD data from polar-orbiting (i.e. MODIS products) and geostationary (i.e. Himawari-8) satellites. In addition, satellite-derived ambient and indoor monitoring $PM_{2.5}$ concentrations might be combined to better delineate the personal-level exposure and evaluate the health impact. Overall, the findings of this study provide comprehensive information about the spatiotemporal exposure patterns to $PM_{2.5}$, which will greatly help to more accurately identify hotspots and evaluate strategies for clean air action.

Disclosure statement

No potential conflict of interest was reported by the author(s).

Funding

Authors contributions

Xia Zhao: Data curation, Methodology, Formal analysis, Visualization, Writing – Original Draft. Yuyu Zhou: Conceptualization, Methodology, Writing – Review & Editing, Supervision. Xi Li: Writing – Review & Editing. Tao Zhang: Resources, Writing – Review & Editing. Yueying Wang: Resources, Methodology, Writing – Review & Editing. Zhengyuan Zhu: Methodology, Writing – Review & Editing. Kai Zhang: Writing – Review & Editing. Deren Li: Writing – Review & Editing.

Data availability statement

The data that support the findings of this study are available from the corresponding author upon reasonable request.

References

Anenberg, S. C., L. W. Horowitz, D. Q. Tong, and J. J. West. 2010. "An Estimate of the Global Burden of Anthropogenic Ozone and Fine Particulate Matter on Premature Human Mortality Using Atmospheric Modeling." *Environmental Health Perspectives* 118 (9): 1189–1195. https://doi.org/10.1289/ehp.0901220.

Bai, H., Y. Shi, M. Seong, W. Gao, and Y. Li. 2022. "Influence of Spatial Resolution on Satellite-Based PM2.5 Estimation: Implications for Health Assessment." *Remote Sensing* 14 (12): 2933. https://doi.org/10.3390/rs14122933.

Bai, H., H. Wu, W. Gao, S. Wang, and Y. Cao. 2023. "Influence of Spatial Resolution of PM2. 5 Concentrations and Population on Health Impact Assessment from 2010 to 2020 in China." *Environmental Pollution* 326:121505. https://doi.org/10.1016/j.envpol.2023.121505.

Bai, K., K. Li, J. Guo, Y. Yang, and N.-B. Chang. 2020. "Filling the Gaps of in situ Hourly PM2.5 Concentration Data with the Aid of Empirical Orthogonal Function Analysis Constrained by Diurnal Cycles." *Atmospheric Measurement Techniques* 13:1213–1226. https://doi.org/10.5194/amt-13-1213-2020.

Beckx, C., L. Int Panis, I. Uljee, T. Arentze, D. Janssens, & G. Wets. 2009. "Disaggregation of Nation-Wide Dynamic Population Exposure Estimates in the Netherlands: Applications of Activity-Based Transport Models." *Atmospheric Environment* 43 (34): 5454–5462. https://doi.org/10.1016/j.atmosenv.2009.07.035.

Brauer, M., G. Freedman, J. Frostad, A. van Donkelaar, R. V. Martin, F. Dentener, R. van Dingenen, et al. 2016. "Ambient Air Pollution Exposure Estimation for the Global Burden of Disease 2013." *Environmental Science & Technology* 50 (1): 79–88. https://doi.org/10.1021/acs.est.5b03709.

Burnett, R., H. Chen, M. Szyszkowicz, N. Fann, B. Hubbell, C. A. Pope 3rd, J. S. Apte, et al. 2018. "Global Estimates of Mortality Associated with Long-Term Exposure to Outdoor Fine Particulate Matter." *Proceedings of the National Academy of Sciences* 115 (38): 9592–9597. https://doi.org/10.1073/pnas.1803222115.

Cao, C., W. Jiang, B. Wang, J. Fang, J. Lang, G. Tian, J. Jiang, and T. F. Zhu. 2014. "Inhalable Microorganisms in Beijing's PM2.5 and PM10 Pollutants During a Severe Smog Event." *Environmental Science & Technology* 48 (3): 1499–1507. https://doi.org/10.1021/es4048472.

Chen, B., Y. Song, T. Jiang, Z. Chen, B. Huang, and B. Xu. 2018. "Real-Time Estimation of Population Exposure to PM2.5 Using Mobile- and Station-Based Big Data." *International Journal of Environmental Research & Public Health* 15 (4): 573. https://doi.org/10.3390/ijerph15040573.

Chen, R., Y. Li, Y. Ma, G. Pan, G. Zeng, X. Xu, B. Chen, and H. Kan. 2011. "Coarse Particles and Mortality in Three Chinese Cities: The China Air Pollution and Health Effects Study (CAPES)." *Science of the Total Environment* 409 (23): 4934–4938. https://doi.org/10.1016/j.scitotenv.2011.08.058.

Chen, Z., B. Yu, Y. Zhou, H. Liu, C. Yang, K. Shi, and J. Wu. 2019. "Mapping Global Urban Areas from 2000 to 2012 Using Time-Series Nighttime Light Data and MODIS Products." *IEEE Journal of Selected Topics in Applied Earth Observations & Remote Sensing* 12 (4): 1143–1153. https://doi.org/10.1109/JSTARS.2019.2900457.

Cheng, N., D. Zhang, Y. Li, X. Xie, Z. Chen, F. Meng, B. Gao, and B. He. 2017. "Spatio-Temporal Variations of PM2. 5 Concentrations and the Evaluation of Emission Reduction Measures During Two Red Air Pollution Alerts in Beijing." *Scientific Reports* 7 (1): 8220. https://doi.org/10.1038/s41598-017-08895-x.

Deville, P., C. Linard, S. Martin, M. Gilbert, F. R. Stevens, A. E. Gaughan, V. D. Blondel, and A. J. Tatem. 2014. "Dynamic Population Mapping Using Mobile Phone Data." *Proceedings of the National Academy of Sciences* 111 (45): 15888–15893. https://doi.org/10.1073/pnas.1408439111.

Dong, Z., H. Wang, P. Yin, L. Wang, R. Chen, W. Fan, Y. Xu, and M. Zhou. 2020. "Time-Weighted Average of Fine Particulate Matter Exposure and Cause-Specific Mortality in China: A Nationwide Analysis." *The Lancet Planetary Health* 4 (8): e343–e351. https://doi.org/10.1016/S2542-5196(20)30164-9.

Du, Y., X. Xu, M. Chu, Y. Guo, and J. Wang. 2016. "Air Particulate Matter and Cardiovascular Disease: The Epidemiological, Biomedical and Clinical Evidence." *Journal of Thoracic Disease* 8 (1): E8–E19. https://doi.org/10.3978/j.issn.2072-1439.2015.11.37.

Fenech, S., R. M. Doherty, C. Heaviside, S. Vardoulakis, H. L. Macintyre, and F. M. O'Connor. 2018. "The Influence of Model Spatial Resolution on Simulated Ozone and Fine Particulate Matter for Europe: Implications for Health Impact Assessments." *Atmospheric Chemistry & Physics* 18 (8): 5765–5784. https://doi.org/10.5194/acp-18-5765-2018.

Gariazzo, C., A. Pelliccioni, and A. Bolignano. 2016. "A Dynamic Urban Air Pollution Population Exposure Assessment Study Using Model and Population Density Data Derived by Mobile Phone Traffic." *Atmospheric Environment* 131:289–300. https://doi.org/10.1016/j.atmosenv.2016.02.011.

Gong, P., X. Li, J. Wang, Y. Bai, B. Chen, T. Hu, X. Liu, et al. 2020. "Annual Maps of Global Artificial Impervious Area (GAIA) Between 1985 and 2018." *Remote Sensing of Environment*: 236. https://doi.org/10.1016/j.rse.2019.111510.

Hamra, G. B., N. Guha, A. Cohen, F. Laden, O. Raaschou-Nielsen, J. M. Samet, P. Vineis, et al. 2014. "Outdoor Particulate Matter Exposure and Lung Cancer: A Systematic Review and Meta-Analysis." *Environmental Health Perspectives* 122 (9): 906–911. https://doi.org/10.1289/ehp.1408092.

Hayes, R. B., C. Lim, Y. Zhang, K. Cromar, Y. Shao, H. R. Reynolds, D. T. Silverman, et al. 2020. "PM2.5 Air Pollution and Cause-Specific Cardiovascular Disease Mortality." *International Journal of Epidemiology* 49 (1): 25–35. https://doi.org/10.1093/ije/dyz114.

He, Q., and B. Huang. 2018. "Satellite-Based High-Resolution PM2.5 Estimation Over the Beijing-Tianjin-Hebei Region of China Using an Improved Geographically and Temporally Weighted Regression Model." *Environmental Pollution* 236:1027–1037. https://doi.org/10.1016/j.envpol.2018.01.053.

Korhonen, A., H. Lehtomäki, I. Karvosenoja, N. Paunu, V. Kupiainen, K. Sofiev, M. Palamarchuk, et al. 2019. "Influence of Spatial Resolution on Population PM2.5 Exposure and Health Impacts." *Air Quality, Atmosphere & Health* 12 (6): 705–718. https://doi.org/10.1007/s11869-019-00690-z.

Krittanawong, C., Y. K. Qadeer, R. B. Hayes, Z. Wang, S. Virani, G. D. Thurston, and C. J. Lavie. 2023. "PM2. 5 and Cardiovascular Health Risks." *Current Problems in Cardiology* 48 (6): 101670. https://doi.org/10.1016/j.cpcardiol.2023.101670.

Lai, M. J., and L. Wang. 2013. "Bivariate Penalized Splines for Regression." *Statistica Sinica* 23:1399–1417. https://doi.org/10.5705/ss.2010.278.

Li, P., X. Guo, J. Jing, W. Hu, W. Q. Wei, X. Qi, and G. Zhuang. 2022. "The Lag Effect of Exposure to PM2.5 on Esophageal Cancer in Urban-Rural Areas Across China." *Environmental Science and Pollution Research International* 29 (3): 4390–4400. Jan. https://doi.org/10.1007/s11356-021-15942-8.

Li, R., Z. Li, W. Gao, W. Ding, Q. Xu, and X. Song. 2015. "Diurnal, Seasonal, and Spatial Variation of PM 2.5 in Beijing." *Science Bulletin* 60 (3): 387–395. https://doi.org/10.1007/s11434-014-0607-9.

Li, T., H. Shen, Q. Yuan, and L. Zhang. 2018. "Validation Approaches for Satellite-Based PM2 5 Estimation: Assessment and a New Approach." arXiv preprint arXiv, 1812.00135. https://arxiv.org/abs/1812.00135.

Li, T., Y. Zhang, J. Wang, D. Xu, Z. Yin, H. Chen, Y. Lv, et al. 2018. "All-Cause Mortality Risk Associated with Long-Term Exposure to Ambient PM2·5 in China: A Cohort Study." *The Lancet Public Health* 3 (10): e470–e477. https://doi.org/10.1016/S2468-2667(18)30144-0.

Li, X., P. Gong, Y. Zhou, J. Wang, Y. Bai, B. Chen, T. Hu, et al. 2020. "Mapping Global Urban Boundaries from the Global Artificial Impervious Area (GAIA) Data." *Environmental*

Research Letters 15 (9): 094044. https://doi.org/10.1088/1748-9326/ab9be3.

Li, X., Y. Zhou, M. Hejazi, M. Wise, C. Vernon, G. Iyer, and W. Chen. 2021. "Global Urban Growth Between 1870 and 2100 from Integrated High Resolution Mapped Data and Urban Dynamic Modeling." *Communications Earth & Environment* 2 (1): 201. https://doi.org/10.1038/s43247-021-00273-w.

Liang, F., Q. Xiao, K. Huang, X. Yang, F. Liu, J. Li, X. Lu, Y. Liu, and D. Gu. 2020. "The 17-Y Spatiotemporal Trend of PM2.5 and Its Mortality Burden in China." *Proceedings of the National Academy of Sciences* 117 (41): 25601–25608. https://doi.org/10.1073/pnas.1919641117.

Lim, C. H., J. Ryu, Y. Choi, S. W. Jeon, and W. K. Lee. 2020. "Understanding Global PM2.5 Concentrations and Their Drivers in Recent Decades (1998–2016)." *Environment International* 144:106011. https://doi.org/10.1016/j.envint.2020.106011.

Liu, M., R. K. Saari, G. Zhou, J. Liu, L. Han, and X. Liu. 2021. "Recent Trends in Premature Mortality and Health Disparities Attributable to Ambient PM2.5 Exposure in China: 2005–2017." *Environmental Pollution* 279:116882. https://doi.org/10.1016/j.envpol.2021.116882.

Lu, X., S. Zhang, J. Xing, Y. Wang, W. Chen, D. Ding, Y. Wu, S. Wang, L. Duan, and J. Hao. 2020. "Progress of Air Pollution Control in China and Its Challenges and Opportunities in the Ecological Civilization Era." *Engineering* 6 (12): 1423–1431. https://doi.org/10.1016/j.eng.2020.03.014.

Luo, G., L. Zhang, X. Hu, and R. Qiu. 2020. "Quantifying Public Health Benefits of PM2.5 Reduction and Spatial Distribution Analysis in China." *Science of Total Environment* 719:137445. https://doi.org/10.1016/j.scitotenv.2020.137445.

Lyapustin, A., and Y. Wang. 2018. *MCD19A2 MODIS/Terra+aqua Land Aerosol Optical Depth Daily L2G Global 1km SIN Grid V006*. Greenbelt, MD, USA: distributed by NASA EOSDIS Land Processes DAAC.

Ma, Z., Y. Liu, Q. Zhao, M. Liu, Y. Zhou, and J. Bi. 2016. "Satellite-Derived High Resolution PM2.5 Concentrations in Yangtze River Delta Region of China Using Improved Linear Mixed Effects Model." *Atmospheric Environment* 133:156–164. https://doi.org/10.1016/j.atmosenv.2016.03.040.

Manning, M. I., R. V. Martin, C. Hasenkopf, J. Flasher, and C. Li. 2018. "Diurnal Patterns in Global Fine Particulate Matter Concentration." *Environmental Science & Technology Letters* 5 (11): 687–691. https://doi.org/10.1021/acs.estlett.8b00573.

Mebrahtu, T. F., G. Santorelli, T. C. Yang, J. Wright, J. Tate, and R. R. McEachan. 2023. "The Effects of Exposure to NO2, PM2.5 and PM10 on Health Service Attendances with Respiratory Illnesses: A Time-Series Analysis." *Environmental Pollution* 333:122123. https://doi.org/10.1016/j.envpol.2023.122123.

MEEPRC. 2016. "Ambient Air Quality Standards (GB3095-2012) Ministry of Ecology and Environment of the People's Republic of China." https://www.mee.gov.cn/ywgz/fgbz/bz/bzwb/dqhjbh/dqhjzlbz/201203/W020120410330232398521.pdf.

Miao, L., S. Tang, Y. Ren, M.-P. Kwan, and K. Zhang. 2022. "Estimation of Daily Ground-Level PM2.5 Concentrations Over the Pearl River Delta Using 1 Km Resolution MODIS AOD Based on Multi-Feature BiLSTM." *Atmospheric Environment* 290:290. https://doi.org/10.1016/j.atmosenv.2022.119362.

Nyhan, M., S. Grauwin, R. Britter, B. Misstear, A. McNabola, F. Laden, S. R. Barrett, and C. Ratti. 2016. ""Exposure Track"—The Impact of Mobile-Device-Based Mobility Patterns on Quantifying Population Exposure to Air Pollution." *Environmental Science & Technology* 50 (17): 9671–9681. https://doi.org/10.1021/acs.est.6b02385.

Orellano, P., J. Reynoso, N. Quaranta, A. Bardach, and A. Ciapponi. 2020. "Short-Term Exposure to Particulate Matter (PM10 and PM2.5), Nitrogen Dioxide (NO2), and Ozone (O3) and All-Cause and Cause-Specific Mortality: Systematic Review and Meta-Analysis." *Environment International* 142:105876. https://doi.org/10.1016/j.envint.2020.105876.

Park, Y. M., and M. P. Kwan. 2017. "Individual Exposure Estimates May Be Erroneous When Spatiotemporal Variability of Air Pollution and Human Mobility are Ignored." *Health & Place* 43:85–94. https://doi.org/10.1016/j.healthplace.2016.10.002.

Parvez, F., and K. Wagstrom. 2020. "Impact of Regional versus Local Resolution Air Quality Modeling on Particulate Matter Exposure Health Impact Assessment." *Air Quality, Atmosphere & Health* 13 (3): 271–279. https://doi.org/10.1007/s11869-019-00786-6.

Pisoni, E., P. Thunis, A. De Meij, J. Wilson, B. Bessagnet, M. Crippa, D. Guizzardi, C. A. Belis, and R. Van Dingenen. 2023. "Modelling the Air Quality Benefits of EU Climate Mitigation Policies Using Two Different PM2. 5-Related Health Impact Methodologies." *Environment International* 172:107760. https://doi.org/10.1016/j.envint.2023.107760.

Pope, C. A., III, and D. W. Dockery. 2006. "Health Effects of Fine Particulate Air Pollution: Lines That Connect." *Journal of the Air & Waste Management Association* 56 (6): 709–742. https://doi.org/10.1080/10473289.2006.10464485.

Pu, Q., and E. H. Yoo. 2022. "A Gap-Filling Hybrid Approach for Hourly PM2.5 Prediction at High Spatial Resolution from Multi-Sourced AOD Data." *Environmental Pollution* 315:120419. https://doi.org/10.1016/j.envpol.2022.120419.

Schwartz, J. 2000. "The Distributed Lag Between Air Pollution and Daily Deaths." *Epidemiology* 11 (3): 320–326. https://doi.org/10.1097/00001648-200005000-00016.

Shi, W., C. Liu, I. Annesi-Maesano, D. Norback, Q. Deng, C. Huang, H. Qian, et al. 2021. "Ambient PM2.5 and Its Chemical Constituents on Lifetime-Ever Pneumonia in Chinese Children: A Multi-Center Study." *Environment International* 146:106176. https://doi.org/10.1016/j.envint.2020.106176.

Shin, M., Y. Kang, S. Park, J. Im, C. Yoo, and L. J. Quackenbush. 2020. "Estimating Ground-Level Particulate Matter Concentrations Using Satellite-Based Data: A Review." *GIScience & Remote Sensing* 57 (2): 174–189. https://doi.org/10.1080/15481603.2019.1703288.

Song, C., J. He, L. Wu, T. Jin, X. Chen, R. Li, P. Ren, L. Zhang, and H. Mao. 2017. "Health Burden Attributable to Ambient PM2.5

in China." *Environmental Pollution* 223:575–586. https://doi.org/10.1016/j.envpol.2017.01.060.

Song, Y., B. Huang, Q. He, B. Chen, J. Wei, and R. Mahmood. 2019. "Dynamic Assessment of PM2.5 Exposure and Health Risk Using Remote Sensing and Geo-Spatial Big Data." *Environmental Pollution* 253:288–296. https://doi.org/10.1016/j.envpol.2019.06.057.

Stanaway, J. D., A. Afshin, E. Gakidou, and S. S. E. A. Lim. 2018. "Global, Regional, and National Comparative Risk Assessment of 84 Behavioural, Environmental and Occupational, and Metabolic Risks or Clusters of Risks for 195 Countries and Territories, 1990–2017: A Systematic Analysis for the Global Burden of Disease Study 2017." *Lancet* 392:1923–1994. https://doi.org/10.1016/S0140-6736(18)32225-6.

Steinle, S., S. Reis, and C. E. Sabel. 2013. "Quantifying Human Exposure to Air Pollution—Moving from Static Monitoring to Spatio-Temporally Resolved Personal Exposure Assessment." *Science of the Total Environment* 443:184–193. https://doi.org/10.1016/j.scitotenv.2012.10.098.

Sun, D., C. Liu, Y. Ding, C. Yu, Y. Guo, D. Sun, Y. Pang, et al. 2023. "Long-Term Exposure to Ambient PM2· 5, Active Commuting, and Farming Activity and Cardiovascular Disease Risk in Adults in China: A Prospective Cohort Study." *The Lancet Planetary Health* 7 (4): e304–e312. https://doi.org/10.1016/S2542-5196(23)00047-5.

Taj, T., A. H. Poulsen, M. Ketzel, C. Geels, J. Brandt, J. H. Christensen, R. Puett, U. A. Hvidtfeldt, M. Sorensen, and O. Raaschou-Nielsen. 2020. "Long-Term Exposure to PM2.5 and Its Constituents and Risk of Non-Hodgkin Lymphoma in Denmark: A Population-Based Case–Control Study." *Environmental Research* 188:109762. https://doi.org/10.1016/j.envres.2020.109762.

Tao, M., J. Wang, R. Li, L. Wang, L. Wang, Z. Wang, J. Tao, H. Che, and L. Chen. 2019. "Performance of MODIS High-Resolution MAIAC Aerosol Algorithm in China: Characterization and Limitation." *Atmospheric Environment* 213:159–169. https://doi.org/10.1016/j.atmosenv.2019.06.004.

Tomar, G., A. S. Nagpure, Y. Jain, and V. Kumar. 2023. "High-Resolution PM2. 5 Emissions and Associated Health Impact Inequalities in an Indian District." *Environmental Science & Technology* 57 (6): 2310–2321. https://doi.org/10.1021/acs.est.2c05636.

Tsou, M. H., H. Zhang, A. Nara, and S. Y. Han. 2018. "Estimating Hourly Population Distribution Change at High Spatiotemporal Resolution in Urban Areas Using Geo-Tagged Tweets, Land Use Data, and Dasymetric Maps." arXiv preprint arXiv, 1810.06554. https://arxiv.org/abs/1810.06554.

Turner, M. C., D. Krewski, C. A. Pope, Y. Chen, S. M. Gapstur, and M. J. Thun. 2011. "Long-Term Ambient Fine Particulate Matter Air Pollution and Lung Cancer in a Large Cohort of Never-Smokers." *American Journal of Respiratory and Critical Care Medicine* 184 (12): 1374–1381. https://doi.org/10.1164/rccm.201106-1011OC.

Wang, X., W. Sun, K. Zheng, X. Ren, and P. Han. 2020. "Estimating Hourly PM2.5 Concentrations Using MODIS 3 Km AOD and an Improved Spatiotemporal Model Over Beijing-Tianjin-Hebei, China." *Atmospheric Environment* 222:222. https://doi.org/10.1016/j.atmosenv.2019.117089.

Wang, Y. 2021. *Next-Generation Functional Data Analysis for Imaging and Spatial Data*. Ames, IA, USA: Iowa State University.

Wang, Y., G. Wang, L. Wang, and R. T. Ogden. 2020. "Simultaneous Confidence Corridors for Mean Functions in Functional Data Analysis of Imaging Data." *Biometrics Bulletin* 76 (2): 427–437. https://doi.org/10.1111/biom.13156.

Wei, J., Z. Li, M. Cribb, W. Huang, W. Xue, L. Sun, J. Guo, et al. 2020. "Improved 1 km Resolution PM$_{2.5}$ Estimates Across China Using Enhanced Space–Time Extremely Randomized Trees." *Atmospheric Chemistry & Physics* 20 (6): 3273–3289. https://doi.org/10.5194/acp-20-3273-2020.

Wei, J., Z. Li, A. Lyapustin, L. Sun, Y. Peng, W. Xue, T. Su, and M. Cribb. 2021. "Reconstructing 1-Km-Resolution High-Quality PM2.5 Data Records from 2000 to 2018 in China: Spatiotemporal Variations and Policy Implications." *Remote Sensing of Environment* 252:112136. https://doi.org/10.1016/j.rse.2020.112136.

Wei, X., K. Bai, N. B. Chang, and W. Gao. 2021. "Multi-Source Hierarchical Data Fusion for High-Resolution AOD Mapping in a Forest Fire Event." *International Journal of Applied Earth Observation and Geoinformation* 102:102366. https://doi.org/10.1016/j.jag.2021.102366.

World Bank Annual Report. 2017. Washington, D.C.: World Bank Group. http://documents.worldbank.org/curated/en/143021506909711004/World-Bank-Annual-Report-2017. (English).

Xiao, Q., F. Liang, M. Ning, Q. Zhang, J. Bi, K. He, Y. Lei, and Y. Liu. 2021. "The Long-Term Trend of PM2.5-Related Mortality in China: The Effects of Source Data Selection." *Chemosphere* 263:127894. https://doi.org/10.1016/j.chemosphere.2020.127894.

Xie, Y., Y. Wang, K. Zhang, W. Dong, B. Lv, and Y. Bai. 2015. "Daily Estimation of Ground-Level PM2.5 Concentrations Over Beijing Using 3 Km Resolution MODIS AOD." *Environmental Science & Technology* 49 (20): 12280–12288. https://doi.org/10.1021/acs.est.5b01413.

Xu, Y., S. Jiang, R. Li, J. Zhang, J. Zhao, S. Abbar, and M. C. González. 2019. "Unraveling Environmental Justice in Ambient PM2.5 Exposure in Beijing: A Big Data Approach." *Computers, Environment and Urban Systems* 75:12–21. https://doi.org/10.1016/j.compenvurbsys.2018.12.006.

Yang, G., Y. Wang, Y. Zeng, G. F. Gao, X. Liang, M. Zhou, X. Wan, et al. 2013. "Rapid Health Transition in China, 1990–2010: Findings from the Global Burden of Disease Study 2010." *Lancet* 381 (9882): 1987–2015. https://doi.org/10.1016/S0140-6736(13)61097-1.

Yin, H., M. Brauer, J. Zhang, W. Cai, S. Navrud, R. Burnett, C. Howard, et al. 2021. "Population Ageing and Deaths Attributable to Ambient PM2· 5 Pollution: A Global Analysis of Economic Cost." *The Lancet Planetary Health* 5 (6): e356–e367. https://doi.org/10.1016/S2542-5196(21)00131-5.

Yin, P., M. Brauer, A. J. Cohen, H. Wang, J. Li, R. T. Burnett, J. D. Stanaway, et al. 2020. "The Effect of Air Pollution on

Deaths, Disease Burden, and Life Expectancy Across China and Its Provinces, 1990–2017: An Analysis for the Global Burden of Disease Study 2017." *The Lancet Planetary Health* 4 (9): e386–e398. https://doi.org/10.1016/S2542-5196(20)30161-3.

Yue, H., C. He, Q. Huang, D. Yin, and B. A. Bryan. 2020. "Stronger Policy Required to Substantially Reduce Deaths from PM2.5 Pollution in China." *Nature Communications* 11 (1): 1462. https://doi.org/10.1038/s41467-020-15319-4.

Zhang, Q., D. G. Streets, G. R. Carmichael, K. B. He, H. Huo, A. Kannari, Z. Klimont, et al. 2009. "Asian Emissions in 2006 for the NASA INTEX-B Mission." *Atmospheric Chemistry & Physics* 9 (14): 5131–5153. https://doi.org/10.5194/acp-9-5131-2009.

Zhang, T., Y. Zhou, K. Zhao, Z. Zhu, G. R. Asrar, and X. Zhao. 2022. "Gap-Filling MODIS Daily Aerosol Optical Depth Products by Developing a Spatiotemporal Fitting Algorithm." *GIScience & Remote Sensing* 59 (1): 762–781. https://doi.org/10.1080/15481603.2022.2060596.

Zhang, X., Y. Chu, Y. Wang, and K. Zhang. 2018. "Predicting Daily PM2.5 Concentrations in Texas Using High-Resolution Satellite Aerosol Optical Depth." *Science of the Total Environment* 631-632:904–911. https://doi.org/10.1016/j.scitotenv.2018.02.255.

Zhao, X., X. Zhang, X. Xu, J. Xu, W. Meng, and W. Pu. 2009. "Seasonal and Diurnal Variations of Ambient PM2.5 Concentration in Urban and Rural Environments in Beijing." *Atmospheric Environment* 43 (18): 2893–2900. https://doi.org/10.1016/j.atmosenv.2009.03.009.

Zhao, X., Y. Zhou, W. Chen, X. Li, X. Li, and D. Li. 2021. "Mapping Hourly Population Dynamics Using Remotely Sensed and Geospatial Data: A Case Study in Beijing, China." *GIScience & Remote Sensing* 58 (5): 717–732. https://doi.org/10.1080/15481603.2021.1935128.

Zheng, T., M. H. Bergin, S. Hu, J. Miller, and D. E. Carlson. 2020. "Estimating Ground-Level PM2.5 Using Micro-Satellite Images by a Convolutional Neural Network and Random Forest Approach." *Atmospheric Environment* 230:230. https://doi.org/10.1016/j.atmosenv.2020.117451.

Zhou, Y., X. Li, G. R. Asrar, S. J. Smith, and M. Imhoff. 2018. "A Global Record of Annual Urban Dynamics (1992–2013) from Nighttime Lights." *Remote Sensing of Environment* 219:206–220. https://doi.org/10.1016/j.rse.2018.10.015.